Proceedings World Geothermal Congress 2020+1
Reykjavik, Iceland, April - October 2021

HEATSTORE: Preliminary Design of a High Temperature Aquifer Thermal Energy Storage (HT-ATES) System in Geneva Based on TH Simulations

Julian E. Mindel and Thomas Driesner

Inst. of Geochemistry and Petrology, Clausiusstrasse 25, 8092 Zürich, Switzerland

julian.mindel@erdw.ethz.ch

Keywords: HEATSTORE, energy storage, numerical analysis, simulation, thermal, hydrological, TH, UTES, HT-ATES

ABSTRACT

Advancing the integration of Underground Thermal Energy Storage (UTES) systems with more traditional energy networks while addressing relevant technical and economic aspects is one of the aims of the European HEATSTORE project with several pilot sites in different countries. Understanding how UTES improves the efficiency of energy use and fits in an otherwise complex system of supply and demand may not be assessed properly without, among other factors, a detailed consideration of the subsurface physics at work.

At the Geneva HEATSTORE pilot site, seasonal storage of up to 50 [GWh/yr] from a waste-to-energy plant into a High Temperature Aquifer Thermal Energy Storage system (HT-ATES) is planned. The Geneva site is arguably the geologically most complex within HEATSTORE as the potential HT-ATES formations are intersected by thrust and strike-slip faults and at least some parts of them display artesian conditions.

In our paper, we developed different operational scenarios that investigate if and how hot water can be stored and produced without significant losses, followed by a numerical analysis to assess HT-ATES options within this complex geological situation. Our simulations are based on a detailed geologic model developed at the University of Geneva and assume a non-mechanically-deforming porous medium subjected to slightly compressible single phase porous media flow with conductive and advective heat transfer. The approach was then used to perform a sensitivity study, while investigating different physical phenomena and their impact on system efficiency.

1. INTRODUCTION

Unused thermal energy produced in times of low demand is often dissipated and lost in our surroundings. The ancient practice of Thermal Energy Storage (TES) is an increasingly popular method of mitigating this loss by addressing the time-dependent supply and demand gaps that exist throughout energy networks worldwide. TES systems are thus critical for the sustainability of a renewables-based energy grid, and their usage frequently results in considerable improvements in terms of energy cost, consumption, and reliability as well as important reductions in CO_2 emissions (Dincer & Rosen, 2011).

Two types of TES exist, typically and respectively defined as *sensible* and *latent* in allusion to the type of heat involved in their operation. Aquifer Thermal Energy Storage (ATES) systems are a subset of the more general *sensible* TES systems, and involve the usage of the thermal and porous capacities of the natural subsurface to store energy via the flow of water at variable temperatures. Although ATES systems may be used equally for cooling or heating, in this work we are particularly concerned with their seasonal usage to store water at relatively high temperatures (HT, ~25 [°C] to ~90 [°C]) sourced during warmer months and delivering the buffered heat to meet the demand of the colder months.

In terms of limitations and as a consequence of their use of the natural subsurface as energy containment, feasibility of ATES systems is heavily reliant on local favorable geology. Water must be used as a working fluid to minimize aquifer chemical contamination, with typical local regulations instructing equal amounts to be injected and produced at all times (Holstenkamp, et al., 2017). Despite these constraints ATES systems have great potential due to their simpler design, high injection and extraction rates, and most importantly due to their large thermal heat capacity at relatively lower costs in comparison to other TES systems that require construction and maintenance of some form of container (Lanahan & Tabares-Velasco, 2017).

The Geneva-section of the HEATSTORE project has set its goals on the assessment of the feasibility of an HT-ATES system to be operated in the Swiss Canton of Geneva. The studied area has been characterized as geologically and logistically challenging (Nawtratil del Bono, et al., 2019) as a result of its prospective aquifers being intersected and offset by faults and the relatively high population density. Given these challenges, using a numerical tool becomes essential to carry out a virtual exploration of possible scenarios. A sensitivity analysis can thus be performed and insight be obtained to characterize response, determine feasibility, and deliver fundamental understanding of the effects of geologic heterogeneities, operational strategies, and groundwater conditions on ATES efficiency. Such a study was carried out previously by (Ingeneurs Résonance, 2017), using a different numerical approach and addressing similar questions regarding the effects of possible parameters via the consideration of a doublet well pattern. It is our intent to contribute and compare to this previously-made analysis, by expanding the parameter space and introducing some of the advantages of simulating Discrete Fracture and Matrix models with a view towards the faulted/fractured complexity of the Geneva basin.

In this paper, we present results and insights obtained during our first design iteration of TH simulations with particular focus on the geology of the Geneva Basin, although the insight obtained may be applicable elsewhere. By using a numerical tool to simulate a large number of scenarios we have worked towards a better understanding of an HT-ATES system response to variations in essential

design factors. Through exploring a multi-dimensional parameter space composed of aquifer thickness, aquifer permeability, well pattern, groundwater flow, dip angle, and the presence of fractures we have produced a range of site-relevant scenarios to be numerically simulated. At the current stage of the Geneva side of the HEATSTORE project, the work was carried out through analysis of TH forward-model simulation results, and our intent is to improve our understanding of the risk involved. Our methodology is described in section 2, while the computational approach is described in section 3. Section 4 presents the results and provides the insight obtained.

2. SIMULATION SCENARIOS

Modern reservoir simulation software capabilities allow us to integrate a considerable level of physical detail to numerical models. Within the HEATSTORE project objectives, a TH reservoir simulator performs as part of a design optimization program, where it essentially replaces the real world system. Ideally, such a program begins with a preliminary storage proposal and input parameters, and within a certain number of cycles the storage design should be improved. In practice, however, the number of possibilities produced by the factors at play and their occasional interdependency can grow unmanageably large rather easily. To ensure success while making our way through towards the TH modelling goals and to minimize the number of design cycles required, we endeavored to address the most fundamentally efficiency-relevant questions:

1. *Buoyancy*: How does aquifer permeability, aquifer thickness, and dip affect efficiency?
2. *Groundwater flow*: How significant is the heat-signature drift?
3. *Fractures*: Will faults, fractures, and other features redirect groundwater flow and/or cause significant energy leaks?
4. *Aquifer thickness*: How much heat is lost to the confining aquitards, and what are the effects on efficiency and environmental impact? How important are screen lengths?
5. *Well pattern*: Are there significant advantages to using a particular pattern?
6. *Combined*: Considering equal amounts of injected and produced volumes, what are the combined effects of all these parameters on the discharged temperature?

Based on these topics, we have developed geologically-based simulation scenarios. We have also narrowed the scope of the resulting and potentially overwhelming combinatorial problem by performing an analysis making simplifying assumptions, using key design factors, and fundamental operational constraints and insight provided by our project partners (de Oliveira, et al., 2017). Each scenario consists in turn of a group of simulation cases (i.e. sub-scenarios), that collectively allow addressing at least one of the fundamental questions. The parameters that may vary within each case include the following:

- Aquifer permeability k and thickness L, and dip.
- Groundwater flow ($\mathbf{v}_{gw}$).
- Number of auxiliary wells and screen length ($L/2$).
- Presence of fractures in two locations: with respect to groundwater flow, upwind and downwind of the storing injector well.

For clarity, in the current design iteration the following variations have not yet been included:

- Volumes, rates, water temperature and/or amount of energy injected.
- Charge, discharge, and storage periods as well as the number of cycles.
- Solid thermal material properties (i.e. specific heat capacity and thermal conductivity)
- Aquifer depth.

Each sub-scenario variant has been assigned a code, and the resulting complete case name can be constructed from the combination of all the respective codes. For example, cases that consider groundwater flow will use the code `YGW`, while the ones that do not, use `NGW`. The table below summarizes the available variations in terms of individual codes. Given the possible combinations of all codes, the total number of simulations to be run is 324. The meaning and values associated to each code is explained throughout this section.

Table 1: Summary of sub-scenario variant codes.

Aquifer Permeability	Aquifer Thickness	Well Strategy	Groundwater	Fracture Configuration	Aquifer Dip
K13	L200	single	YGW	F0	FLAT
5K13	L300	doublet	NGW	FU	INCL
K12	L400	5spot		FD	

2.1 Geometrical-Geological Model

Based on the detailed gelogical study carried out by the University of Geneva (UniGe) and Services Industriels de Genève (SIG) (see Figure 1), a cube-shaped 1 km^3 geological model was constructed by UniGe using the original analysis of a collection of subsurface datasets. The latter included 2-D seismic reflection data, petrophysical data, and well reports from the recently drilled GEO-01 well. The analysis was coupled to the interpretation of data available from the GEOMOL 3D Project (Bayerisches Landesamt für Umwelt, n.d.) (Swiss Federal Office of Topography, n.d.) , where a 3D geological model of the Geneva area can be extracted. All horizons were initially considered as horizontal surfaces, simplifying structures in preparation for simulation work, however a dip angle of 15º was introduced in the simulation scenarios to include its possible effects on the thermal efficiency.

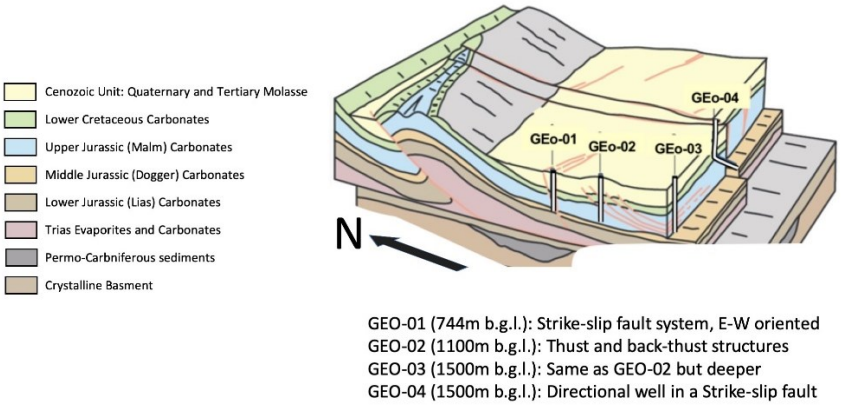

Figure 1: Illustration of the local geology, locations and targets of the planned GEO-series wells in the Geneva basin (modified from (Nawtratil del Bono, et al., 2019))

While keeping the supplied material properties in mind, we have further simplified the model geometry to the basic necessary elements for an ATES, consisting of a single permeable aquifer rock layer confined between two layers with lower permeability and porosity (see Figure 2). This characteristic and idealized configuration tends to prevent heat and fluid loss, as well as heat contamination to the surroundings (Dincer & Rosen, 2011), and its simplification was assumed sufficient for a first design iteration given the relatively large amount of simulations needed. As part of one of the possible variants, we have also introduced a model containing a 15° dip angle (see Figure 2(c)).

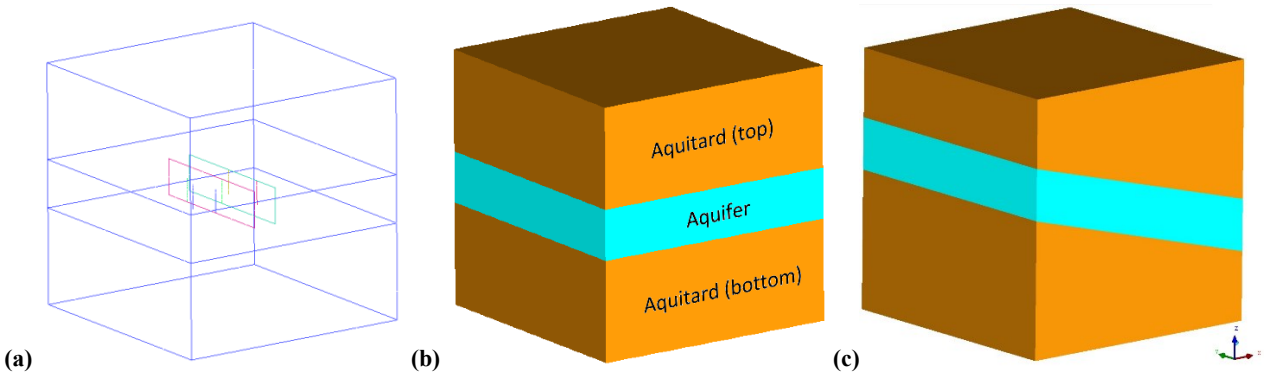

Figure 2: Geometrical/Geological model representing the basic elements of an ATES, depicting (a) possible well and fracture locations, (b) a flat version of the model, and (c) a version of the model possessing an aquifer with a 15º angle of dip.

Analysis of 2D reflection seismic data has revealed a considerable presence of fault corridors in the studied area, and since their role is still uncertain (Rousillon, 2018) they could be acting as groundwater channels, or have become impermeable obstacles and compartmentalized target aquifers. Basing ourselves on an initial groundwater measurement carried out at the well GEO-01 of 20 [m/yr] and measured values of permeability, we have chosen to take a moderately conservative approach in our groundwater velocity value assumptions (i.e. 2 [m/yr]).

Material and groundwater flow parameters obtained from the geological interpretations and measurements were provided by UniGe and SIG to be used in the simplified model for the simulations. A summary of the values used, including permeability and thickness values related for variants K13, 5K13, K12, L200, L300, and L400 is presented in Table 2.

2.1.1 Fractures

Due to the geologic setting, it is likely that aquifers within the studied area are fractured and offset. The surrounding topography, major thrust and strike-slip faults, and the fact that throughout the the Cenozoic interval the most important faults often present themselves in a flower structure (Charollais, et al., 2007) (Angelillo, 1987), make a fracture/faulted setting very likely. Furthermore, the planned a prospective GEO-02 well is scheduled to reach 1100 [m] in depth, drilling into a reef complex associated to a sequence of thrust faults. Although smaller-scale fractures and cracks may improve the permeability of the aquifer formations, the evident presence of larger ones increases the need to consider fractures and faults explicitly in our simulation models.

As shown in Table 2, smaller scale fractures and cracks are taken into accound via an “effective” matrix porosity and permeability in the aquifer region. In terms of scenario variants, the modelled option F0 denotes a model without any other explicit fractures. Using the ground water flow direction as a reference, a single fracture is located 50 [m] in front or *Upwind* of GW_1 (i.e. the main charging well) for variant FU , while an identical fracture set 50 [m] behind or *Downwind* of GW_1 for variant FD. These last two cases implement a single fracture as a zone of specific assumed width and properties (also shown in Table 2) and therefore while porosity is high, it is not equal to 1, which would be the case for a perfectly void fracture.

Table 2: Summary rock material parameters (Driesner, T. (ed.), 2019)

Parameter	Units	Aquitard (top)	Aquifer	Aquitard (bottom)
Density (ρ_r)	[kg/m^3]	2450	2450	2680
Permeability (k) (original matrix)	[m^2]	10^{-17}	10^{-15}	10^{-17}
Permeability K13 (k) (fractured, effective)	[m^2]	10^{-17}	10^{-13}	10^{-17}
Permeability 5K13 (k) (fractured, effective)	[m^2]	10^{-17}	$5{\cdot}10^{-13}$	10^{-17}
Permeability K12 (k) (fractured, effective)	[m^2]	10^{-17}	10^{-12}	10^{-17}
Porosity (ϕ) (matrix, effective)	[-]	0.01	0.2	0.01
Permeability (k) (fracture, effective)	[m^2]	N/A	10^{-11}	N/A
Porosity (ϕ) (fracture, effective)	[-]	N/A	0.5	N/A
Fracture thickness	[m]	N/A	0.1	N/A
Specific Heat Capacity ($c_{p,r}$)	[J/(Kg·K)]	860.2	832.9	849.9
Thermal Conductivity λ_r (λ_r)	[W/(m·K)]	2.275	2.806	2.692
Thickness L200 (L)	[m]	400	200	400
Thickness L300 (L)	[m]	350	300	350
Thickness L400 (L)	[m]	200	400	400
Groundwater velocity (v_{gw}) (assumed)	[m/yr]	N/A	2	N/A

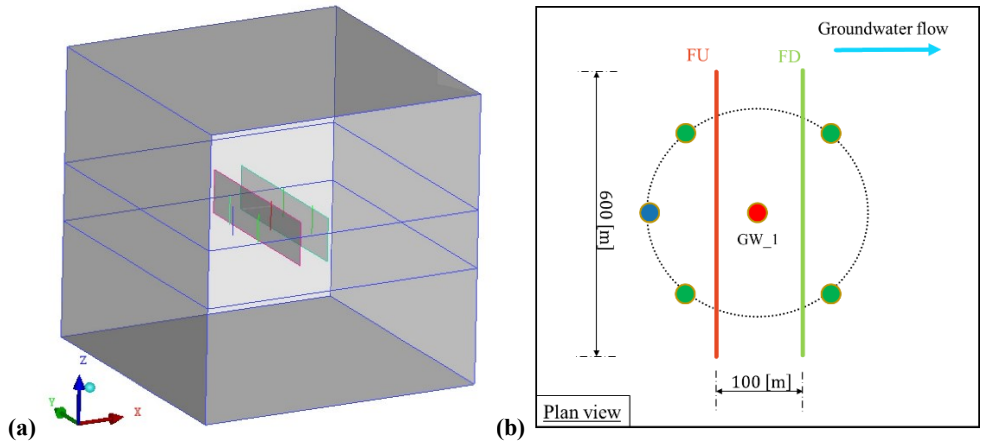

Figure 3: (a) Three dimensional geological model depicting fracture locations used in the simulations and (b) their specific x-y plane view location with respect to the wells.

2.2 Operational design

The HT-ATES system will be integrated into Geneva's district heating network through the Les Cheneviers incineration plant (Driesner, T. (ed.), 2019), and thus some reasonably accurate input can be obtained to run predictive models over its projected lifetime. Thermal power output from the waste incineration plant, demand, and temporal load/unload cycles over a one year time frame were provided by UniGe and SIG based on SIG's district heating systems development plan (Services Industriels de Genève, 2019). With this information we obtained the necessary parameters for all the simulation configurations needed.

Table 3: Summary of basic input parameters.

Total Energy to Inject (E_{GWh}) (per year cycle)	50 [GWh]
Temperature of injection (T_i)	90 [℃]
Period of injection/charge (t_c)	120 [days]
Period of production/discharge (t_d)	120 [days]
Period of storage (2) ($t_{s,1}$, $t_{s,2}$)	60 [days], 65.25 [days]
Volume injected (V_i)	622080 [m^3]
HT-ATES life time	15 [yr]

The basic operational yearly cycle strategy consists of a period of continuous charge for 120 [days], followed by storage for 60 [days], discharge for 120 [days], and further storage for 65.25 [days]. A basic average volumetric flow rate q_V can be determined by first calculating the total volume of water V_i at T_i necessary to deliver E_{GWh}, and dividing it by the charge time period,

$$V_i = \frac{E_{GWh}}{\rho_f c_{p,f} \Delta T} \qquad q_V = \frac{V_i}{t_c}\left[\frac{\mathrm{m}^3}{\mathrm{s}}\right] \tag{1}$$

Where $c_{p,f}$ and ρ_f are the isobaric specific heat and density of the fluid. The temperature change ΔT in this case is the difference between T_i and the original water temperature before it was heated at the waste incinerator plant (ΔT is assumed 70 [°C]). It is useful then to estimate the hydraulic r_w and thermal r_{th} radii of an ideal cylinder of aquifer rock (Bloemendal & Hartog, 2018), given by

$$\pi r_w^2 L\phi = V_i \rightarrow r_w = \sqrt{\frac{V_i}{\pi L \phi}} \qquad r_{th} = \sqrt{V_i \frac{c_{p,f}\rho_f}{\pi L\left(c_{p,f}\rho_f \phi + c_{p,r}\rho_r(1-\phi)\right)}} \tag{2}$$

Given the porosity ϕ, specific heat capacity $c_{p,r}$ and density ρ_r provided for the aquifer rock, equations shown in (2) can be plotted together as a function of the aquifer thickness L.

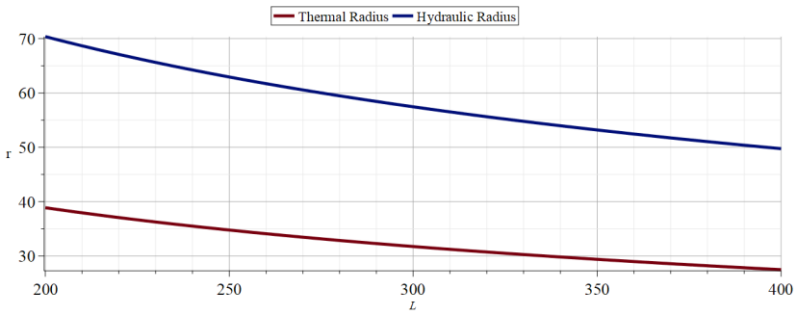

Figure 4: Hydraulic (red) and thermal (blue) radii as a function of aquifer thickness (L)

Based on Figure 4, to prevent the thermal front from reaching the auxiliary wells (Ganguly & Mohan Kumar, 2015), and assuming the possibility of a single, a doublet, and a 5-spot well strategy, a basic table of essential simulation input parameters was developed and is presented in Table 4. Recommendations for well spacing in the literature vary between a single thermal radius r_{th} and three thermal radii, and consequently an intermediate value was chosen.

Table 4: Summary well-strategy-based simulation configuration parameters.

Scenario variant code	Radial distance from centre well [m]	Main well flow rate [m³/s] inj/prod	Aux. well flow rate [m³/s] inj/prod
single	N/A	0.06/-0.06	N/A
doublet	141	0.06/-0.06	0.06/-0.06
5spot	141	0.06/-0.06	0.015/-0.015

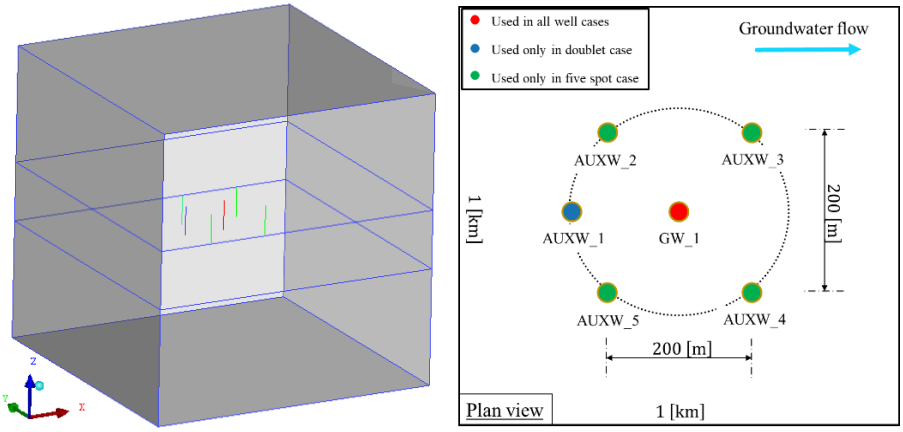

Figure 5: Well pattern (a) 3D design, and (b) plan view of their locations and names.

A basic well design and the corresponding well names to be used in each scenario variant corresponding to well strategy, can be observed in Figure 5. The 'single' case assumes that an auxiliary well exists to satisfy environmental re-injection requirements, but it is sufficiently far from the main well so that its effects can be neglected. For any particular simulation, all wells involved are fully vertical and have the same screen length, which is vertically centered on the aquifer layer. The screen length was designed as one half of the aquifer thickness.

3. COMPUTATIONAL APPROACH

In contrast to typical free flow conditions of fluids above the ground, subsurface fluids tend to percolate through the rock pore space as well as larger spaces such as fractures and faults. As a result, the classic mathematical description of fluid momentum may be heavily simplified to a balance between viscous and gravitational forces known as Darcy's Law by neglecting inertia effects and assuming a linear relationship between viscous forces and flow velocity. In terms of the simulation goals at hand, these simplifications are notably needed, given that the loss in mathematical complexity and non-linearity is more than compensated for by underground material heterogeneity.

The TH conceptual model neglects rock structural-mechanic (M) and fluid/rock chemical processes (C), and thus focuses on providing a first basic understanding of plausible fluid flow (H) and heat transfer (T) conditions. This means that the concept would allow the modelling of injection of a buoyant compressible percolating fluid that is able to exchange heat with its surroundings via advection and conduction processes. It is, however, not aimed at representing effects such as the thermal expansion of the rock surrounding the fluid, fracture mechanical/chemical sealing/opening, and chemical permeability alteration.

To further reduce complexity and aid computational effort, the model also assumes that only one single phase fluid occupies the totality of the void space available in the rock. This results in an averaged rock-fluid bulk material which is the essence of porous media assumptions and also allows for further simplifications such as the assumption of an averaged flow velocity (i.e. Darcy velocity) existing over an arbitrary representative portion of the domain, the instantaneous thermal equilibrium between fluid and rock, and the subdivision of the heat transport mechanisms. The advective heat transport is thus assumed to be performed by the fluid, while conductive heat transport is performed mainly by the rock material, depending on local porosity.

To use an accurate equation of state for water and capture any buoyancy effects as well as transient pressure effects resulting from changes in operation modes as accurately as possible, we also allow fluid density, enthalpy, and heat capacity to be functions of pressure and temperature (IAPWS, 2018). This renders the resulting set of partial differential equations (PDEs) with non-linear characteristics.

Considering that the material properties of the porous rock to be isotropic, locally uniform (i.e. to a minimum discrete level of a computational cell), and constant, the governing equations that represent our assumptions are dictated by classic (Bear, 1972) conservation laws of mass (3), momentum (4) simplified to Darcy's Law, and the decoupled advective and conductive energy transport (5) and (6). These are expressed in cartesian coordinates via:

$$\frac{\partial(\rho_f \phi)}{\partial t} + \nabla \cdot (\rho_f \mathbf{v}) + q_{\rho,f} = 0 \tag{3}$$

$$\mathbf{v} = -\frac{k}{\mu}(\nabla p - \rho_f \mathbf{g}) \tag{4}$$

$$\frac{\partial(\phi \rho_f h_f)}{\partial t} + \nabla \cdot (\rho_f h_f \mathbf{v}) + q_h = 0 \tag{5}$$

$$C_{p,t}\frac{\partial T}{\partial t} - \nabla \cdot (\lambda_t \nabla T) = 0 \tag{6}$$

where t is time, ρ_f is the fluid density, ϕ is the porosity, $\mathbf{v}$ is the Darcy flow velocity vector, $q_{\rho,f}$ represents fluid mass sources and sinks, p is the fluid pressure, $\mathbf{g}$ is the gravitational acceleration vector, k is the rock permeability, and μ is the fluid viscosity. Equations (5) and (6) conform the law of conservation of energy, and heat is transported via advection only by the fluid (5) and by conduction via a combination of the rock and the fluid (6). We purposely neglect kinetic, potential, and viscous dissipation effects, h_f is the specific enthalpy of the fluid, $C_{p,t}$ is the volumetric bulk heat capacity, T is the bulk temperature, λ_t is the bulk thermal conductivity where $\lambda_t = \lambda_w \phi + \lambda_r (1-\phi)$, and q_h represents heat sources and sinks. It is important to note that both rock and water conducitivities λ_r and λ_w are assumed constant, and that we also opt at this stage to ignore effects of salinity transport. The latter feature is available in the simulator if expectations of its effect on the system become of greater concern.

A numerical discretization approach based on a combined Finite Element (FE) and Finite Volume (FV) (Paluszny, et al., 2007) methodologies is used on equations (3) to (6) to create a solution algorithm. Equations (3) and (5) are spatially discretized using a hybrid method of FE and FV, while equation (6) and a restructured version of equation (3) into a pressure equation are based purely on FE. Equation (4) is essentially a post-process operation for velocity calculation and it can be evaluated after the solution of each timestep using FE shape functions. Time is discretized into a sequence of *timesteps* assuming a linear variation of all properties within any particular timestep. The combination of FE and FV formulations allow for the use of unstructured meshes (i.e. an irregular tessellation of elements), which in turn allows for a greater computational efficiency when capturing geometrical and solution detail. Each simulation performs a sequence of calculations during each timestep while following an algorithm that was transformed into C++ code using the combined Nexus.sim and CSMP++ frameworks. The code was compiled into a cross-platform (Windows, Linux, Mac OS) application via a variety of compilers (i.e. Intel, GNU, Clang, etc.).

3.1 Discrete Geometric Representation

TH simulations require a computational grid based on an arbitrarily-detailed geometry. The geometrical model volume is thus tessellated by unstructured/irregular tetrahedrons, honouring material interfaces between rock-types, fractures, and well trajectories. Triangles are used to tessellate lower dimensional representations (i.e. interior surfaces) of fractures, and line segments to tessellate well completions. The latter triangles and line segments are often referred to as LDE's (Lower Dimensional Elements), since they possess at least one dimension lower than the maximum dimension used to represent the global domain. The resulting complete tessellation (i.e. also named grid or mesh) can be seen in Figure 6, and is populated with all known material properties via the simulator application, honouring the information provided by the studies described in Section 2.1.

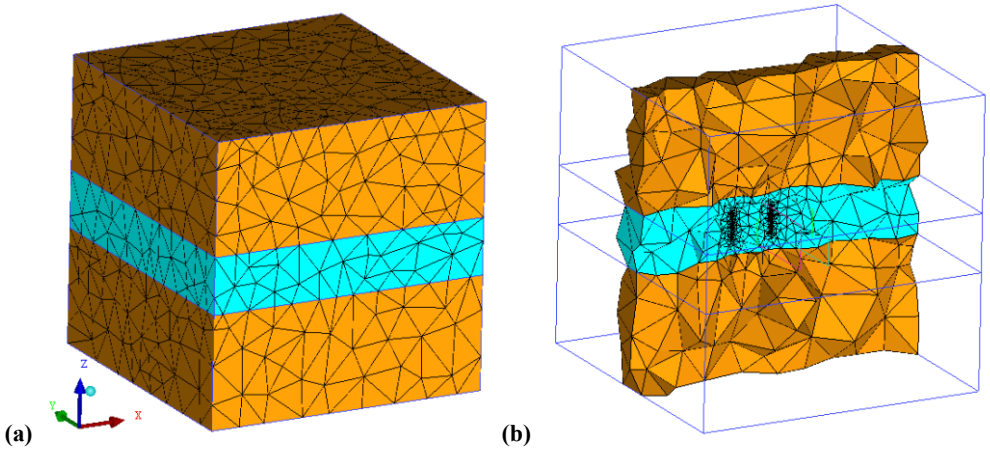

Figure 6: (a) Volumetric tetrahedral tesselation of the geometrical model using the ICEMCFD software, and (b) mesh cutplane depicting variable resolution when approaching regions containing wells.

3.2 Essential Conditions

Partial differential equations (3) to (6) form a non-linear, coupled, initial and boundary value problem. To provide *closure* to this problem, boundary and initial conditions need to be supplied to obtain the desired time-sequence of unique solutions. Initial conditions are defined by the values of the main solution variables (i.e. pressure, temperature) and associated function-variables (i.e. density, specific enthalpy, heat capacity, sources and sinks) at the beginning of the simulation ($t = 0$) for the entire simulated domain. In the case of boundary conditions, we have used the *Dirichlet* type to impose the value of a variable at the boundary, and the *Neumann* type to impose a normal gradient or flux of a variable. For both initial and boundary conditions, imposed values may be *x, y, z* coordinate-dependent, while boundary conditions may also be time-varying. Other conditions similar to the Dirichlet condition are applied within the domain to control sources and sinks, which represent the wells in operation. Adiabatic conditions, also known as *natural* in relation to the applied FE and FV methods, are assumed for all boundaries parallel to the modelled groundwater flow direction.

To achieve the intial groundwater flow conditions we must solve a steady state problem based on equations (3) and (6). To achieve this we define a reference surface condition of temperature and pressure at depth 0 [m] . Values for lateral hydrostatic boundary conditions are obtained, and an extra pressure based on the groundwater hydraulic head is added only to one of the boundaries (i.e the inlet) where the negative normal matches the groundwater flow direction. The boundary conditions are then fixed throughout the transient part of the simulation. A summary of the applied conditions is provided in Table 5.

Table 5: Summary of essential conditions applied during initialization and transient simulation. Unless specified, boundary locations not mentioned are assumed to be set to the *Natural* condiction for a particular variable.

Variable	Type (location)	Value or function	Applied During	Comment
Pressure	Dirichlet (top boundary)	101325 [Pa]	Initialization	All other boundaries set to *natural* conditions (no-flow)
Pressure	Dirichlet (inlet and outlet boundaries)	Hydrostatic	Initialization and Simulation	In the YGW case, it includes groundwater pressure at the inlet boundary.
Temperature	Dirichlet (top boundary)	10 ºC	Initialization and transient simulation	Constant surface temperature condition.
Temperature	Neumann (bottom boundary)	Heatflux 0.064 [W/m^2]	Initialization and transient simulation	Heat flux is converted to a temperature gradient via the fluid and rock thermal conductivity values adjacent to the boundary.
Enthalpy and Fluid Density	Inflow/Outflow (inlet and outlet boundaries)	Functions of *p* and *T*, depending on flow direction and upwind values	Transient simulation	Allows entry and exit of mass and enthalpy on boundaries of the domain without the need to set a *Dirichlet* condition for outflux.

4. RESULTS AND DISCUSSION

We obtained results for 324 simulations produced by the combinations of simulation variant codes provided in Table 1. To assess the effects of the varying parameters on the cyclic efficiency using this relatively large volume of data, we applied an exergetic analysis for the HT-ATES expected life time. This type of analysis is favorable with respect to an energetic basis, since it accounts for the temperature at which water is produced from the aquifer (Dincer & Rosen, 2011). For reference, the energy efficiency η_{En} of an ATES system is given by

$$\eta_{En} = \frac{\int_{t_d} \left\{ \int_{\Omega_{GW\_1}} q_{h,out} d\Omega \right\} dt}{\int_{t_c} \left\{ \int_{\Omega_{GW\_1}} q_{h,in} d\Omega \right\} dt} \tag{7}$$

where Ω_{GW_1} is the volume immediately surrounding the well, $q_{h,in}$ and $q_{h,out}$ are the only enthalpic sources and sinks present within Ω_{GW_1} during charging and discharging, respectively, t_c is the charging time, and t_d is the discharge time. Exergy is a measure of the theoretical maximum amount of work that could be extracted from the flow, and is comparable to Carnot's efficiency of a reversible heat engine. Exergy efficiency η_{Ex} may be calculated in a similar fashion to η_{En},

$$\eta_{Ex} = \frac{\int_{t_d} \left\{ \int_{\Omega_{GW\_1}} q_{h,out} \left(1 - \frac{T_{ref}}{T}\right) d\Omega \right\} dt}{\int_{t_c} \left\{ \int_{\Omega_{GW\_1}} q_{h,in} \left(1 - \frac{T_{ref}}{T_i}\right) d\Omega \right\} dt} \tag{8}$$

where T is the temperature measured at the well, T_i is the injection temperature, T_{ref} is a reference temperature (i.e. both in Kelvin in this case), such as the original environmental temperature of the aquifer before its use as an ATES, or a threshold temperature below which the exergy input and output is assumed not useful to produce work. Exergy efficiency tends to be lower than energy efficiency in ATES systems, given that as T approaches T_{ref} the exergy contribution approaches zero. If $T < T_{ref}$ at any point in time, the amount of exergy for that period is negative. As a result, the amount of energy input, stored, and discharged from the ATES will only be *useful*, or of good enough *quality*, as long as the temperature of the flow can be maintained above T_{ref}. Over subsequent cycles and theoretically depending on the discharge time and overall length of each cycle, the exergy lost to the aquifer surroundings results in an increase of the temperature near the well at the end of each cycle, thus increasing η_{En} and η_{Ex} over time as shown in Figure 7.

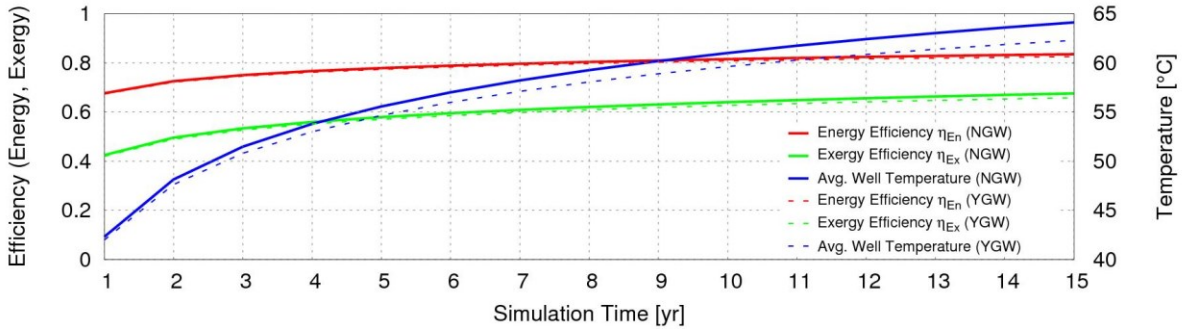

Figure 7: Energy and Exergy efficiency variation with time for the expected ATES lifetime comparing a case with and without groundwater flow: 'L400_K13_5spot_NGW_F0_FLAT', and 'L400_K13_5spot_YGW_F0_FLAT'. The right-hand axis depicts temperature measurement at well GW_1 for the end of each cycle.

Given our observation that efficiencies increase monotonically over time, we found it practical to use the values for the last cycle as a measure of performance for our analyses. A summary exergy efficiency values at the end of life of the ATES for each of 324 simulations is presented in Figure 8, using a reference temperature T_{ref} of 50 [°C] or 323.15 [K].

4.1 Aquifer Permeability and Thickness (K13, 5K13, K12, L200, L300, L400)

Results shown in Figure 8(a) display a significant performance increase with decreasing permeability, where improvements range between 2% to 4%. This can be attributed to the fact that if we assume equal screen length ($L/2$), flow velocities to be similar due to equal injection rates, and that injection pressures are not a mechanical issue, then the lower permeability allows for a better containment of energy during the storage periods. Higher permeabilities allow the heat signature to be more mobile and particularly subjected to drift due to buoyancy and groundwater effects. Buoyancy effects can be observed in further detail through Figure 9(a), (d), and (g), where three simulations differ only with respect to aquifer permeability.

For the thicknesses considered in this study, Figure 8(b) shows a consistent increase of exergy efficiency with decreasing thickness, where improvements can range from 0.5% to 3%. If we once more consider uniform injection rates across simulations and a screen length of $L/2$, a thicker aquifer decreases the injection flow rate per meter of screen length and thus the necessary injection pressure. Nevertheless, it also decreases the thermal radius r_{th} and thus shifts the location of the heat loss from a vertical one into the confining layers to a lateral one into the aquifer surroundings (see Figure 9(a), (b), and (c)). More heat may thus be lost due to both conduction and convection within the aquifer, as can be noticed in Figure 9(i).

The case of permeability and thickness highlights a main issue with ATES systems in which the optimal condition for flow where less injection pressure is needed for the same injection rate, conflicts with the optimal conditions for energy containment.

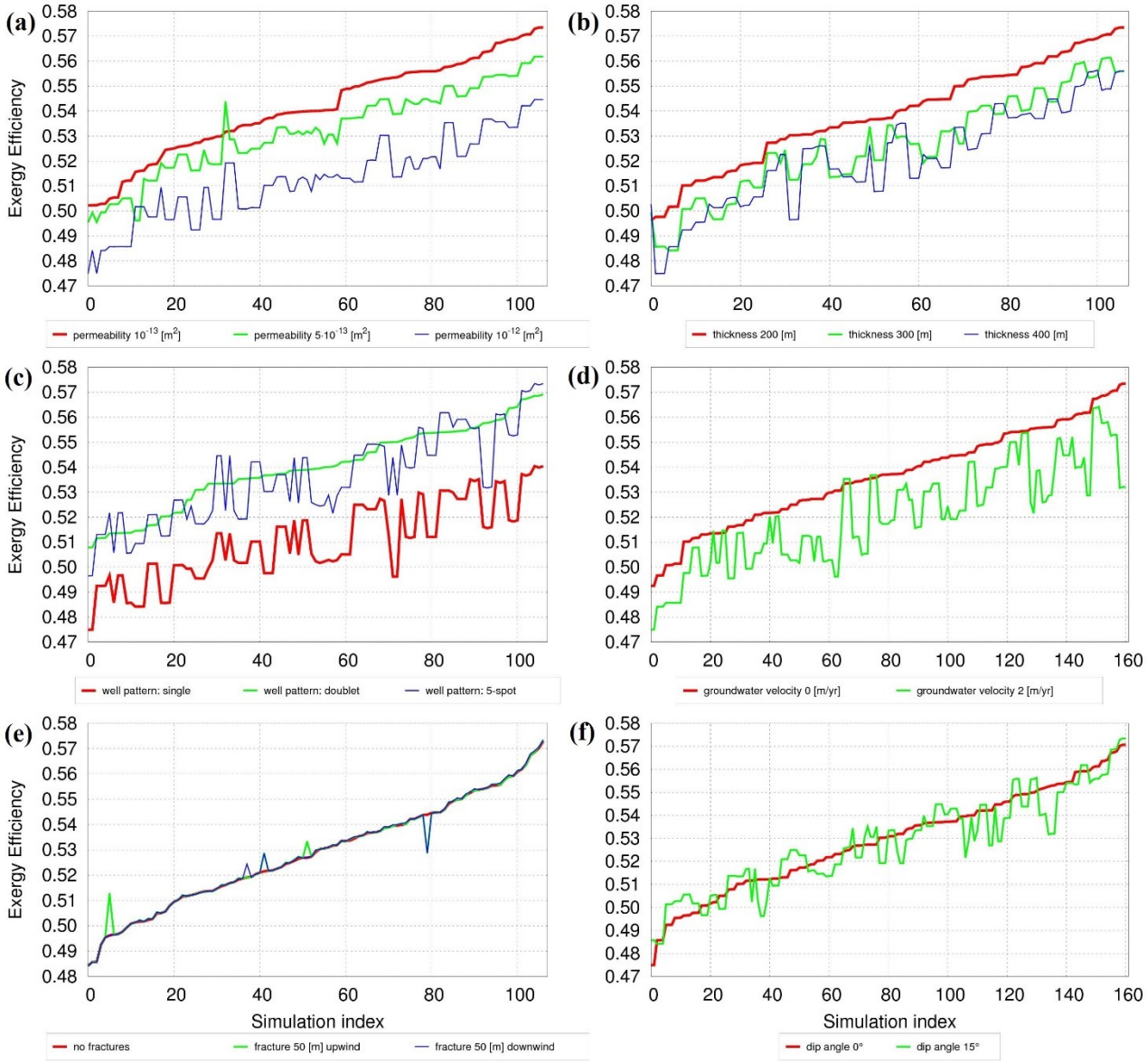

Figure 8: Exergy efficiency measured at the end of the ATES lifetime. Each graph represents a particular horizontal ordering of the same set of results, sorted in increasing exergy efficiency w.r.t. a particular variant code (see Table 1). The simulation index is an arbitrary number guide pointing to a subset of otherwise identical simulations that only differ by one particular parameter: (a) aquifer permeability, (b) aquifer thickness, (c) well pattern, (d) groundwater velocity, (e) fracture configuration, and (f) aquifer dip angle.

4.2 Well Pattern and Groundwater flow (single, doublet, 5spot, NGW, YGW)

Our results show that presence and proximity of auxiliary wells is essential to the performance of an ATES system. Figure 8(c) shows that the single well pattern, which also models the case for which auxiliary wells are markedly far away to provide pressure support, is consistently outperformed by the doublet and 5-spot patterns. In turn, the 5-spot pattern outperforms the doublet somewhat marginally in only some of the cases. From a cost-effectiveness point of view, the doublet pattern appears to be superior. Snapshots of the simulation results using each pattern can be observed in the columns of Figure 10.

As shown in Figure 8(d) performance of the ATES is affected negatively in general, and by up to 4% in some cases due to introduction of groundwater flow at 2 [m/yr]. This is mainly caused by the heat signature tending to drift away from the wells due to advective transport by the groundwater current, as can be observed comparing the two rows of simulations in Figure 10.

4.3 Fracture Configuration and Aquifer Dip Angle (F0, FU, FD, FLAT, INCL)

Fracture configurations chosen for this study show negligible effects on efficiency, as evidenced by the frequently overlapping curves in Figure 8(e), even though the fractures are within 50 [m] of the GW_1 and auxiliary wells. Our initial assessment points towards the fracture permeability and thickness being considered low and the fractures not being close enough to GW_1 or any of the auxiliary wells. This result warrants further study of fracture configurations to be tested, most likely in a separate form due to the practically limitless number of realizations possible.

Some sensitivity to aquifer dip angle does appear to exist, as can be observed in Figure 8(f). Nevertheless, a clear effect cannot be established without a further, and more detailed study. Sensitivity might be higher for aquifers that are thinner than 200 [m], which is the lowest value used in this study.

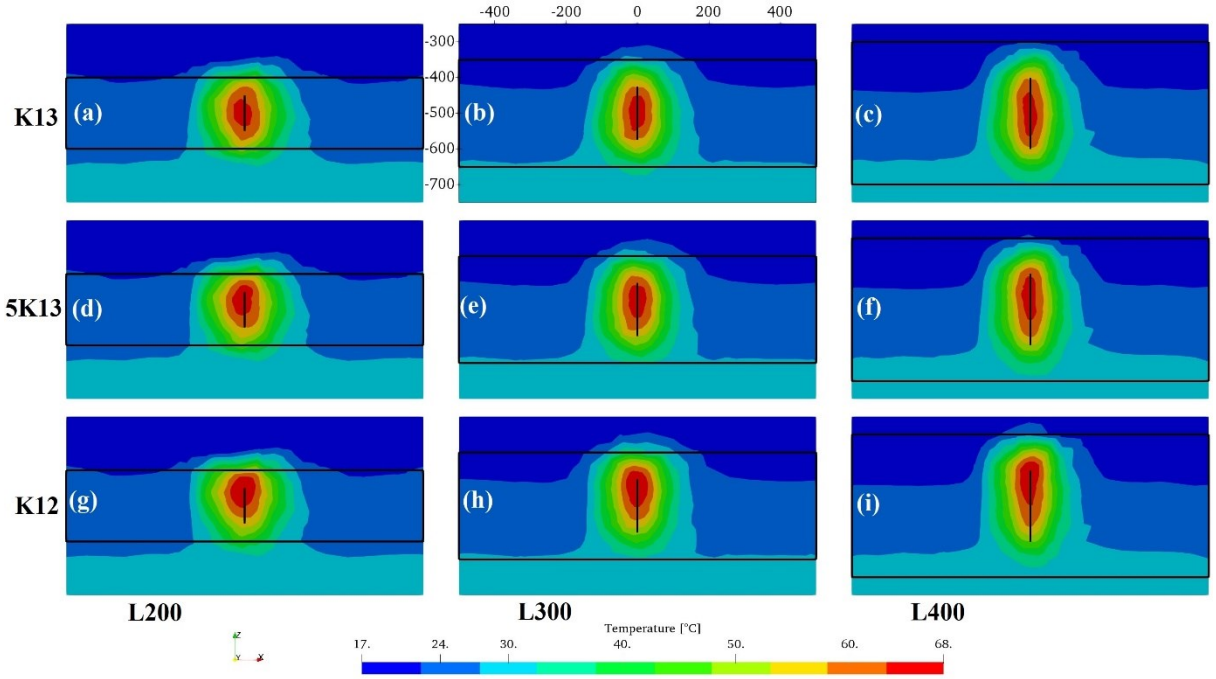

Figure 9: Temperature plots through the middle x-z plane (i.e. vertical) of the domain for 9 simulations with no inclination (FLAT), no groundwater flow (NGW), equal well pattern (single), and no fractures (F0), at the end of year 15 depicting the effects of permeability and thickness on ATES performance. Row-wise, K13 (a,b,c), 5K13 (d,e,f), and K12(g,h,i) permeabilities have been applied to the top, middle and bottom rows respectively, while column-wise, L200 (a,d,g), L300 (b,e,h), and L400 (c,f,i) have been applied to the left, middle and right columns of simulations, respectively. The vertical domain has been trimmed up to between -250 and -750 [m].

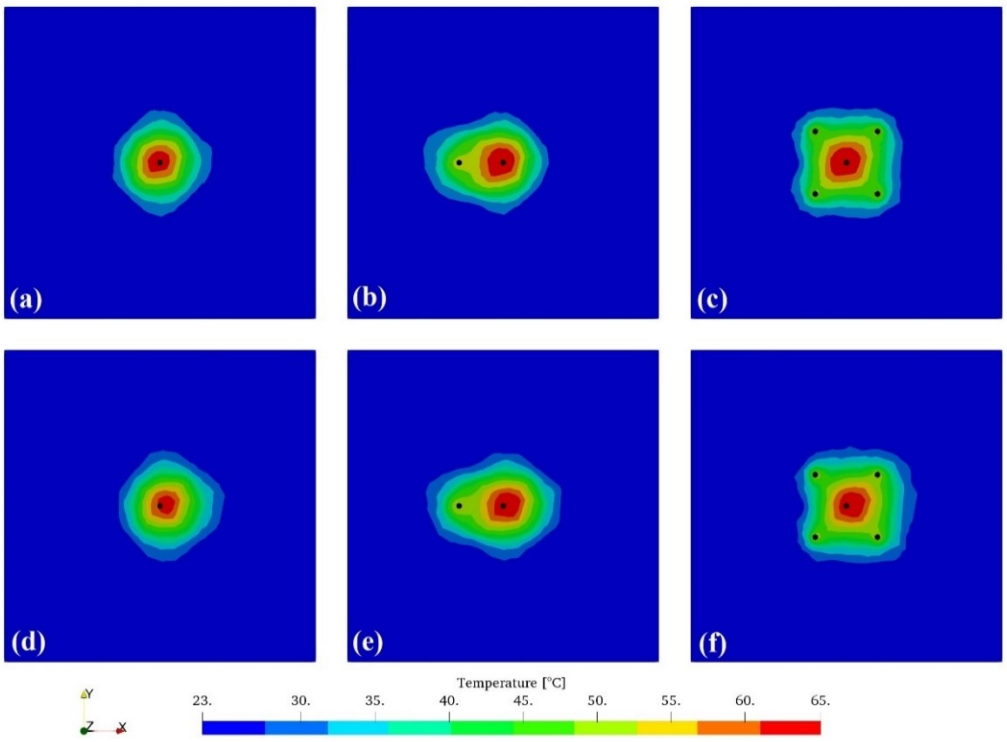

Figure 10: Well pattern and groundwater effects on the temperature signature at the end of the ATES lifetime in a full-domain middle x-y planar cross section for 6 simulations with no inclination (FLAT), no fractures (F0), equal permeability (K12), and equal thickness (L200). Row-wise, NGW (a,b,c), and YGW (d,e,f), groundwater conditions have been applied to the top, and bottom rows respectively, while column-wise, single (a,d), doublet (b,e), and 5spot (c,f) have been applied to the left, middle and right columns of simulations, respectively.

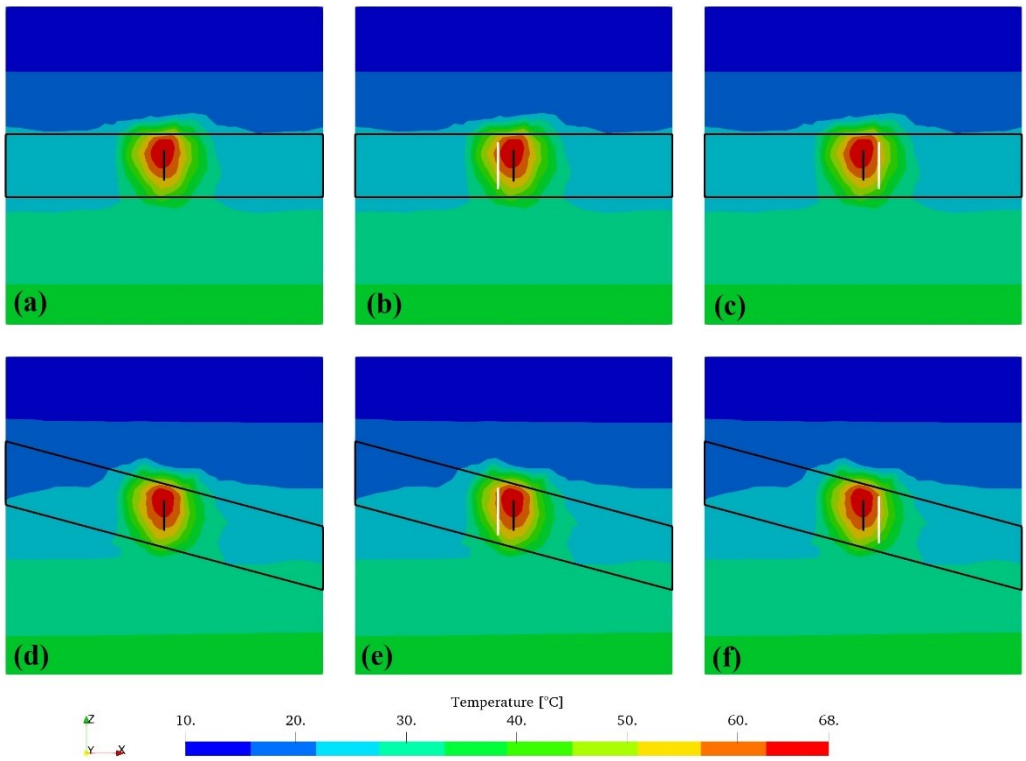

Figure 11: Fracture configuration and aquifer dip angle effects on the temperature signature at the end of the ATES lifetime in a full-domain middle x-z planar (i.e. vertical) cross section for 6 simulations with equal permeability (K12), equal thickness (L200), equal well pattern (single), and no groundwater flow (NGW). Row-wise, FLAT (a,b,c), and INCL (d,e,f), diap angle conditions have been applied to the top, and bottom rows respectively, while column-wise, F0 (a,d), FU (b,e), and FD (c,f) fracture configurations have been applied to the left, middle and right columns of simulations, respectively. Well GW_1 and aquifer perimeter are demarcated by black lines, while fractures are shown as white lines.

5. CONCLUSIONS

We have carried out a numerical study of various HT-ATES system realizations based on parameters of aquifer permeability, aquifer thickness, well pattern, groundwater conditions, dip angle, and fracture configurations. By simplifying an originally complex geological situation, we obtained a series of scenarios aimed at a fundamental understanding of how ATES systems respond to their settings and surroundings, and how to best design them. Considering the geology, material properties, fluid properties, and industry-based operational conditions we have also investigated the plausibility storing hot water and recovering it at the maximum temperature possible via an exergetic analysis of a large number of simulations.

Our study further confirms some observations that have already been made in the literature, particularly with respect to groundwater drift and buoyancy effects present in high permeability aquifers. We have also observed that when active, auxiliary wells help mitigate pressure-peak related effects, improve the thermal front sweep, and also provide some measure of shielding against the drift due to the flow of groundwater.

In particular, we observed that although a permeability design sweet-spot could be numerically found for a particular geologic/geometric configuration, the design process is rather driven by the geo-availability in the prospective site, thus highlighting the importance of a thorough and continued (hydro-)geological study. In a similar light, lower aquifer thicknesses seem to be a favorable configuration, although to inject an equal amount of energy through a water volume rate at the same temperature, higher injection pressures are required which may impose mechanical limitations. Furthermore, particularly in terms of simulations when flow-rate values are equivalent, permeabilities do impose a numerical limitation since resulting injection and production pressure values can be unrealistically high and low, respectively. Further work should be carried out in expanding this study, particularly to better contextualize the geological configurations with particular emphasis on fractures and faults, analyze the effects of aquifer depth, and assess the influence of surface temperature conditions.

AKNOWLEDGEMENTS

This work was supported by the HEATSTORE project, and is also a contribution to the national Swiss research program SCCER SoE.

HEATSTORE (170153-4401) is one of nine projects under the GEOTHERMICA – ERA NET Cofund aimed at accelerating the uptake of geothermal energy in Europe. The project is subsidized through the ERANET cofund GEOTHERMICA (Project n. 731117) by the European Commission, RVO (the Netherlands), DETEC (Switzerland), FZJ-PtJ (Germany), ADEME (France), EUDP (Denmark), Rannis (Iceland), VEA (Belgium), FRCT (Portugal), and MINECO (Spain). More information is available via http://www.heatstore.eu .

The aim of the SCCER-SoE is to carry out innovative and sustainable research in the areas of geo-energy and hydropower. As a national network, the SCCER-SoE brings together expertise from 25 Swiss scientific institutions, industrial enterprises, and federal agencies. Its activities are undertaken in coordination with the Swiss Federal Office of Energy. The SCCER-SoE is financed by the Swiss National Science Foundation and the Commission for Technology and Innovation. The latter is also responsible for the supervision of the SCCER-SoE. More information is available via http://www.sccer-soe.ch .

6. REFERENCES

Angelillo, V., 1987. *Les marnes et grès gris à gypse ("molasse grise") du bassin genevois. Diploma thesis..* Unpublished ed. Geneva: Univ. of Geneva.

Bayerisches Landesamt für Umwelt, n.d. *GeoMol: Assessing subsurface potentials of the Alpine Foreland Basins for sustainable planning and use of natural resources.* [Online] Available at: http://www.geomol.eu/home/index_html

Bear, J., 1972. *Dynamics of Fluids in Porous Media.* New York: Dover Publications.

Bloemendal, M. & Hartog, N., 2018. Analysis of the impact of storage conditions on the thermal recovery efficiency of low-temperature ATES systems. *Geothermics,,* Volume 71, pp. 306-319.

Charollais, J. et al., 2007. La Molasse du basin franco-genevois et son substratum. *Arch.Sci.,* Issue 60, pp. 59-174.

de Oliveira, F. et al., 2017. Spatial and temporal characterization of energy demand and resources for an existing and dense urban district in Geneva. *Energy Procedia,* Volume 122, pp. 259-264.

Dincer, I. & Rosen, M., 2011. *Thermal Energy Storage Case Studies.* 2nd ed. s.l.:John Wiley & Sons, Ltd.

Driesner, T. (ed.), 2019. *Initial report on tools and workflows for simulating subsurface dynamics of different types of High Temperature Underground Thermal Energy Storage,* Zurich: GEOTHERMICA – ERA NET Cofund Geothermal, unpublished report.

Ganguly, S. & Mohan Kumar, M., 2015. A numerical model for transient temperature distribution in an Aquifer Thermal Energy Storage system with multiple wells. *Lowland Technology International,* Volume 17.

Holstenkamp, L. et al., 2017. Interdisciplinary Review of Medium-deep Aquifer Thermal Energy Storage in North Germany. *Energy Procedia,* Volume 135, pp. 327-336.

IAPWS, 2018. *The IAPWS Formulation 1995 for the Thermodynamic Properties of Ordinary Water Substance for General and Scientific Use (IAPWS R6-95(2018)),* Prague, Czech Republic: International Association for the Properties of Water and Steam.

Ingeneurs Résonance, 2017. *Stockage de chaleur dans le Malm du bassin genevois. ÉTUDE DU COMPORTEMENT THERMO-HYDRAULIQUE D'UN SYSTÈME HT-ATES EN AQUIFÈRE PROFOND.,* s.l.: Rapport technique TR-6001.031/NL.

Lanahan, M. & Tabares-Velasco, P., 2017. Seasonal Thermal-Energy Storage: A Critical Review on BTES Systems, Modeling, and System Design for Higher System Efficiency. *Energies,* 10(6).

Nawtratil del Bono, C., Meyer, M. & Martin, F., 2019. *GEothermie 2020: Avancée du programme et premiers succès. Presentation Journée Romande de Geothermie 2019,* Lausanne: SIG.

Paluszny, A., Matthaei, S. K. & Hohmeyer, M., 2007. Hybrid finite element–finite volume discretization of complex geologic structures and a new simulation workflow demonstrated on fractured rocks. *Geofluids,* p. 186–208.

Rousillon, E., 2018. *Characterisation and rock typing of deep geothermal reservoirs in the Greater Geneva Basin (Switzerland & France). Doctoral Thesis. no Sc. 5196.* Geneva: University of Geneva.

Services Industriels de Genève, 2019. *The heart of the SIG strategy.* [Online] Available at: https://ww2.sig-ge.ch/en/a-propos-de-sig/nos-engagements/transition-energetique [Accessed July 2019].

Swiss Federal Office of Topography, n.d. *Switzerland in 3D.* [Online] Available at: https://www.swisstopo.admin.ch/en/home.html